applied sciences

MDPI

Article

Central Composite Design Optimisation of Banana Peels/Magnetite for Anaerobic Biogas Production from Wastewater

Jeremiah A. Adedeji *, Emmanuel Kweinor Tetteh, Gloria Amo-Duodu, Edward Kwaku Armah, Sudesh Rathilal and Maggie Chetty

Green Engineering and Sustainability Research Group, Department of Chemical Engineering, Faculty of Engineering and The Built Environment, Durban University of Technology, Durban 4001, South Africa

* Correspondence: jerry_4real@live.com

Abstract: Biogas production from wastewater as a function to curb waste and provide energy security has gained worldwide attention. Ensuring the stability of anaerobic digestion (AD) of physiochemical and biological complexity necessitates optimization. In this study, a central composite design (CCD) from a response surface methodology (RSM) was employed to evaluate and optimize the effects of bio-stimulation of banana peels coupled with magnetite on the anaerobic digestion of wastewater to produce biogas. An experimental matrix of 14 runs using the CCD, with two factors (nanoparticle and biochar load) as a function of pH, biogas production, and COD removal by the AD process was operated at a constant mesophilic temperature (37 °C) for 28 days. The analysis of variance (ANOVA) showed that the quadratic models attained were significant (p-values < 0.05) with a high coefficient of determination (R^2) values closer to 1. The optimized conditions, including nanoparticle (0.46 g) and biochar (0.66 mgVS/L), resulted in biogas production (19.26 mL/day), pH (7.07), and COD removal (75.17%). This suggests 100% desirability at a 95% confidence level. This finding depicts the trade-off between biogas productivity, biodegradability, and stability of the AD process established for future consideration of using nanoparticles as bio-stimulant.

Keywords: anaerobic digestion; banana peel; biochemical methane potential; biosorbent; biochar; response surface methodology

Citation: Adedeji, J.A.; Tetteh, E.K.; Amo-Duodu, G.; Armah, E.K.; Rathilal, S.; Chetty, M. Central Composite Design Optimisation of Banana Peels/Magnetite for Anaerobic Biogas Production from Wastewater. *Appl. Sci.* **2022**, *12*, 12037. https://doi.org/10.3390/app122312037

Academic Editor: Dino Musmarra

Received: 20 October 2022
Accepted: 20 November 2022
Published: 24 November 2022

1. Introduction

A renewable and eco-friendly alternative energy source comes in handy as today's energy demand surges. Anaerobic digestion (AD) has been one of the most important techniques that convert organic waste into renewable energy in the form of methane (CH_4) -enriched biogas [1]. This has been ascribed to its efficacy in reducing high-concentration organic wastewater streams and producing renewable energy, notably hydrogen and methane [2,3]. The most intriguing aspect of AD is that it enables the simultaneous digestion of multiple substrates as well as the addition of other additives to enhance the process [4].

A very promising developing technology that offers intriguing advantages over the conventional AD process is the treatment of wastewater employing a bio-stimulated anaerobic process using nanoparticles [5]. This technology has a strong capacity for breaking down concentrated and durable materials, making it profitable for producing valuable biogas. For instance, iron (Fe)-based NPs become essential additives to the microorganisms.

Iron additives used as NPs have a higher surface-to-volume ratio, a larger specific surface area, and higher surface reactivity, allowing them to be used to eliminate a broader range of inhibitory properties and pollutant species in wastewater treatment, such as high ammonia, phosphorus, and sulphate concentrations, as well as excessive

amounts of heavy metal [6–9]. Due to their low cost, high conductivity, and reactivity, as well as their ability to release metallic nutrients for anaerobic microorganisms, nano-sized irons, as well as their oxides and other composites, are the most widely used nano-additives for optimizing the performance of an anaerobic digester for wastewater with a low to medium biodegradability index [7,10–13].

Food waste accounts for a large component of municipal solid waste, with almost 1.3 billion tons of food waste created globally each year [13]. It is anticipated that this amount will rise much more in the coming years. As a result of its heavy consumption, fruit waste, such as peels and seeds, is generated. The disposal of these wastes has become an issue globally [14]. For example, banana peels are usually thrown instead of being consumed by livestock. This has led to their conversion into biochar for other useful purposes [15,16]. Biochar, a precursor to activated carbon, is a solid carbonaceous material formed when biomass is thermochemically converted in an oxygen-depleted environment [17]. Numerous wastes, including agricultural wastes such as fruit and vegetable wastes [18], animal manure [19], wood [20], and sewage sludge [21], can be used as feedstocks for biogas production. Since the effects of iron nanoparticles (magnetite) and biochar have been documented independently, examining the synergetic effect of iron nanoparticles and biochar generated from a banana peel as an AD bio-stimulator comes in handy.

The major mechanisms underlying biochar's efficacy are its favourable physicochemical properties, such as a high cations exchange capacity, large porosity, and surface area, which enable surface complexation for the interaction with nutrient cycles, mineral precipitation for immobilization or adsorption, and modified symbiotic relationships between microbial communities [22,23]. Thus, biochar supplementation is an alternate strategy for enhancing the metabolic activity of anaerobic microbes involved in the AD process [24,25]. Studies have shown that biochar could significantly reduce the lag phase, increase methane production, and relieve inhibitor stress during the AD process [26–28]. As a result, an attempt to optimize biochemical processes in maximizing efficiency eludes the principles of the third rule of thermodynamics.

In the biotechnology sector, process optimization for industrial operations has shown a significant impact on maximizing finished products. In this case, an increase in biogas production and quality (methane content increment and CO_2 reduction) involves complex biological and physiochemical reactions [29,30]. Aside from the microbial and enzymatic catalytic effect of converting organic waste into biogas (hydrolysis, acetogenesis, acidogenesis, and methanogenesis), other factors can also influence AD efficiency. These operating parameters, such as pH, alkalinity, retention time, temperature, feedstock, and organic loading, collectively influence biogas production [31]. To avoid process instability, failure, and operational interruptions, the use of a response surface methodology (RSM) has played an important role in modelling and predicting AD process dynamics.

Response surface methodology (RSM) is a mathematical and statistical set of techniques that can be used to design and develop empirical models and estimate the optimal conditions and their impact on a process. The designs of RSM include Central Composite design (CCD), Box-Behnken design (BBD), Full factorial, and Optimal designs. Among them, the CCD, made up of three levels (two-level full or fractional design and central points), augmented by star point ($\pm\alpha$), is used for experimental design for fitting polynomial equations. As a result, the star point gives more flexibility for an experimental design by estimating the curvature. Therefore, this study employed RSM CCD to investigate the synergistic effect of adding banana peels coupled with magnetite to the process of biogas production from wastewater. The AD process was operated under a mesophilic temperature of 35°C and with digestion lasting for 28 days, with biogas production and chemical oxygen demand (COD) removal as output responses.

2. Materials and Methods

2.1. Sample Collection

This study made use of banana peels, iron nanoparticles, and sewage sludge for the AD process. A local South African wastewater treatment plant based in Amanzimtoti, KwaZulu-Natal Province, supplied the wastewater sample used in this study. APHA [29]. The samples were taken immediately after the primary settling tank, and the samples' temperature and pH were determined on-site using a pH meter equipped with a temperature sensor (Ohaus Corporation, Parsippany, NJ, USA). The inoculum was anaerobically digested sludge from an existing anaerobic digester at the same wastewater treatment plant. At the time of sampling, the digester at the plant was operating at a temperature of 25 °C, and the pH of the inoculum was 7.19. On the same day, the samples were also analysed for total solids (204.5 mgTS/L) and volatile solids (106 mgVS/L) before being preserved at 4 °C in the research laboratory's cold room. Prior to the experimental runs, the initial COD (2380 ± 57.6 mg/L), colour (57 ± 12.5 Pt. Co), turbidity (17.3 ± 24.6 NTU), and pH (6.59 ± 1.3) of the wastewater were recorded. 3M of NaOH(aq) was used to adsorb any CO_2 that might be produced, and gas samples were taken once a week for analysis. The COD and colour were characterized using a spectrophotometer (HACH, DR 3900 (Düsseldorf, Germany). The turbidity was analysed using a turbidimeter (Hach, 2100N (Loveland, CO, USA).

2.2. Biochar Preparation

Bananas were acquired at a local South African market, and the banana peels were then oven dried at 60 °C till bone dried. The banana peel-derived biochar (Bi) was made to calcine for 1 h at a furnace temperature of 800 °C [30,31].

2.3. Nano-Particle Preparation

The magnetite NPs (MNPs) used were prepared in-house according to co-precipitation techniques [32,33], with detailed characteristics reported in [30,31]. Before the preparation of the MNPs, magnetite (Fe_3O_4) was prepared in a single-step mode. In a 2 L beaker, a precursor solution was poured containing a 1:1 volume ratio (0.5 L/0.5 L) of Fe^{3+} and Fe^{2+} solutions. The pH was adjusted by dropwise addition of 2 mL surfactant to the mixture (Fe^{3+}/Fe^{2+}), and the pH was reduced to 2 and a microemulsion formed. An amount of 250 mL of 3M NaOH was added dropwise to the mixture. Continuous stirring (15 rpm) resulted in the formation of a thick black precipitate with a pH range of 10–12. The precipitate formed was then heated to 70 °C for 2 h (aging) and then allowed to cool to room temperature. The resultant solids were washed three times with distilled water and ethanol, and the supernatant was discarded. Following that, the precipitate was oven dried for 12 h at 80 °C, followed by 1 h of calcination at 550 °C.

2.4. Biochemical Potential Test

The batch digesters were made up of 1 L glass Schott bottles. The inoculum (300 mL) and the substrate (500 mL) were stored in each AD reactor, which was sealed with a screw cap. Three organic loading ratios (0.5, 1, 1.5) were used for the biochar under mesophilic (37 ± 1 °C) conditions for 28 days to measure the methane production. Mixing each sample for 3 min before AD resulted in a homogeneous mixture, and the batch experiments were conducted under nitrogen gas with flushed conditions for 3 min to promote AD. The systems in all the reactors were shaken manually for 2 min daily during the AD process. Duplicate sample analysis was done for all samples.

2.5. Experimental Design

Using a data-driven approach and RSM, 14 experiment runs were designed using CCD. Two factors considered were nanoparticle (0.2–0.6 g) and biochar (0.5–1.5) loading with respect to pH, biogas production, and COD removal as responses. Subjecting the

alpha levels to full-face centred the two factors considered a subject of interest, which, because of our previous studies [31], was carried out using a one-factor-at-a-time approach. The experimental runs of the CCD matrix were simulated using the Design-Expert (11) software (version 13.05, StateEase, Minneapolis, MN, USA). This enabled the identification of interaction effects, process optimization, and maximization of biogas production. The response surface was estimated using a quadratic polynomial model, as shown by Ghaleb et al. [34].

3. Results and Discussion

3.1. Anaerobic Digested Wastewater Performance

The obtained output data represent the impact of the input factor and microbial stability of the anaerobically digested wastewater for biogas production. Using the RSM-derived CCD matrix of 14 experimental runs, the response data were modelled as a function of the input variables. Table 1 presents the experimental and predicted results of pH, biogas production, and COD removal. Aside from the experimental data fitted on mathematical models, the basis of the RSM optimization of the independent variables was determined by maximizing the AD process. Response graphs of the interactive effect of the input variables were obtained via the analysis of variance in the experimental results fitted on the models. The models were verified, and the optimal conditions obtained for the highest possible desirability were established.

Table 1. Central composite design matrix with experimental and predicted results.

Run	A: Nanoparticle Load (g)	B: Biochar Load (mg Vs)	pH		Daily Biogas Production (mL/day)		COD Reduction (%)	
			Actual	Predicted	Actual	Predicted	Actual	Predicted
1	0.2	0.5	6.79	6.78	3.32	3.54	76.04	76.34
2	0.4	0.5	7.06	7.06	11.59	11.42	78.33	78.41
3	0.6	1	7.14	7.17	23.68	23.51	69.31	69.64
4	0.6	1	7.2	7.17	23.68	23.51	69.31	69.64
5	0.6	1.5	7.24	7.23	8.84	9.07	68.9	68.7
6	0.4	1.5	7	7.04	12.11	11.83	69.68	69.51
7	0.4	1	7.02	7.02	24.45	23.89	70.33	70.93
8	0.2	1.5	7.22	7.22	8.39	8.73	65.91	66.46
9	0.2	1	6.87	6.87	18.68	18.40	68.8	68.375
10	0.6	0.5	7	6.99	13.32	13.43	77.07	76.62
11	0.4	1.5	7.08	7.04	12.11	11.83	69.68	69.51
12	0.2	1	6.87	6.87	18.68	18.40	68.8	68.38
13	0.4	1	7.02	7.01	22.45	23.89	71.33	70.93
14	0.4	0.5	7.06	7.06	11.59	11.42	78.33	78.41

3.1.1. pH Performance

The treated effluent was eluded, and the AD methanogenesis was operated within a pH range between 6.8 and 7.3. After the response pH range (Figure 1) was obtained, it was observed that the stability of the AD process was based on the acidogenesis and methanogenesis activity of the microbes. Herein, the mean pH (7) shown in Figure 1 indicates the neutrality and stability of the bioreactor. The variation of pH in a few experiments might be due to the self-buffering of the pH and the gradual degradation of the organic content of the wastewater into biogas. This confirms that the biogas produced from the conversion of the acetate and CO_2 might have utilized the extra H^+ or OH^- radical ions, which caused the pH variation [35]. Additionally, the alkalinity and basicity of the substrate affect the protonation and deprotonation of oxygen-containing groups in the biochar and nanoparticle additives [36]. Here, the pH recorded reveals the degree of influence of ionization of the charged species of the substrate that favoured methanogenesis and biogas production. This confirms that an anion adsorption surface becomes positively

charged when the surface is negatively charged at pH values above the potential zero charges of the cation favourable to methanogenic activity [32,37,38].

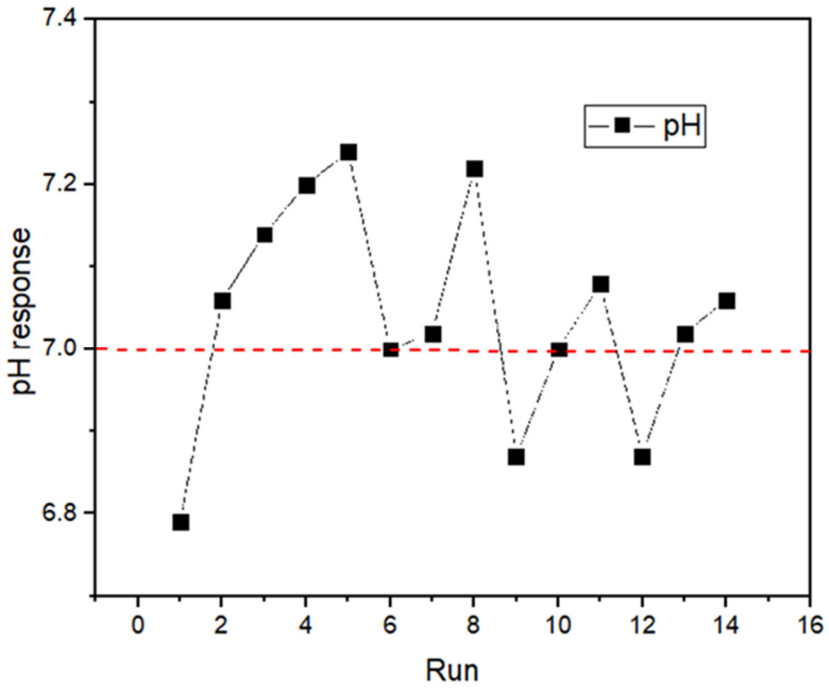

Figure 1. pH response per CCD experimental run.

3.1.2. Biogas and COD Removal Performance

The biodegradation of the organic content of the wastewater in the generation of biogas was monitored. The efficiency of COD removal was used to ascertain the efficiency of the methanogenesis phase of the bioreactors at different nanoparticle and biochar loads. It was deduced that the degradation of the organic substrate by the microorganism increased the percentage of COD removal and biogas production [30,39,40]. The COD removal observed was between the range of 65–78%, whereas the biogas was also within a range of 3–25 mL/day. However, the biogas production was variable over time and never reached a true steady state. This was due to the variation in the organic content (COD) and enzymatic reactions in the bioreactor. The low biogas production and COD removal recorded in some of the runs (Figure 2) might be due to the lag phase of microbial growth in the batch-conditioned reactor. Further, the high biogas production and COD removal recorded may be attributed to the exponential growth of the methanogens with respect to an acclimatized time rate. This indicates the high levels of organic matter (COD) being consumed by the methanogenic microorganism for growth, resulting in the conversion into biogas production [41–43].

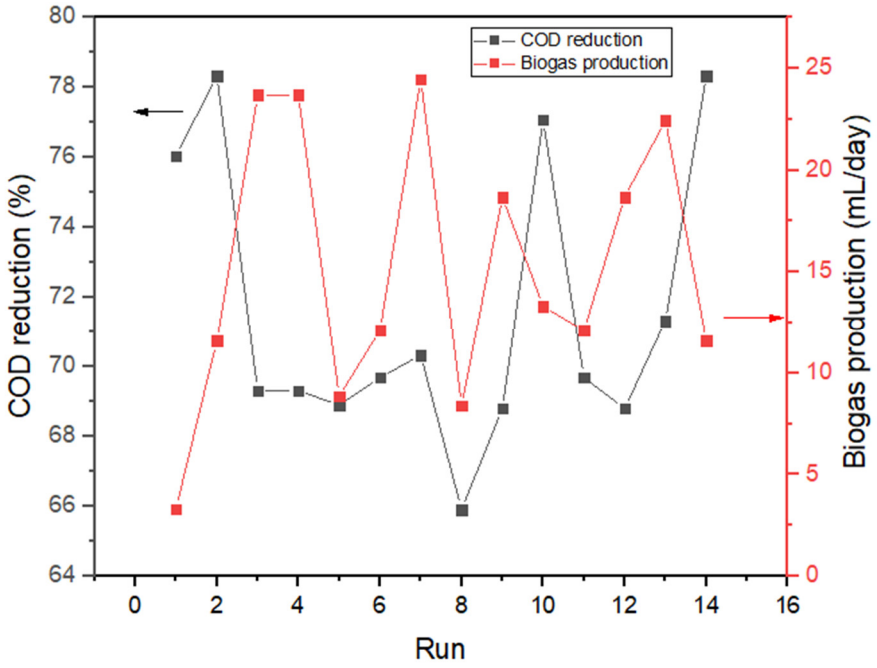

Figure 2. COD removal (%) response per CCD experimental run.

3.2. Modelling and Analysis of Variance(ANOVA)

The data obtained from the CCD experimental matrix (Table 1) was statistically modelled using a multifunctional selection at a 95% confidence level and *p*-values of <0.05 [44]. This was done to graphically determine the influential and interactive effect of the input variables on the responses. The model equations, in terms of the actual terms expressed in (1)–(3), are a reduced form of a quadratic model obtained after the rejection of insignificant terms with *p*-values > 0.05. The negative and positive signs before the model terms, respectively, represent the antagonistic and synergistic effects on the responses. Here, the interaction (AB) effective between the nanoparticle load (A) and biochar load (B) had a significant impact on all the responses (pH, biogas production, and COD removal) and the model's predictability concerning the responses for each given level of the input factors for the experimental runs (Figure 3). It was observed that the regression coefficients were highly significant and scaled to accommodate each unit factor intercept. Further, the closeness of the model-predicted results to the diagonal line illustrated the precision and accuracy of the models [45–47].

$$\mathrm{pH} = 6 + 6.325\mathrm{A} - 0.19\mathrm{B} - 3.875\mathrm{AB} - 8.68\mathrm{A}^2 + 0.89\mathrm{B}^2 + 8.87\mathrm{A}^2\mathrm{B} - 1.85\mathrm{AB}^2 \quad (1)$$

$$\text{Biogas production} = -51.97 + 95.31\mathrm{A} + 108.08\mathrm{B} - 23.85\mathrm{AB} - 73.34\mathrm{A}^2 - 49\mathrm{B}^2 \quad (2)$$

$$\text{COD removal} = 84.93 + 36.75\mathrm{A} - 35.06\mathrm{B} + 4.9\mathrm{AB} - 48.12\mathrm{A}^2 + 12.1\mathrm{B}^2 \quad (3)$$

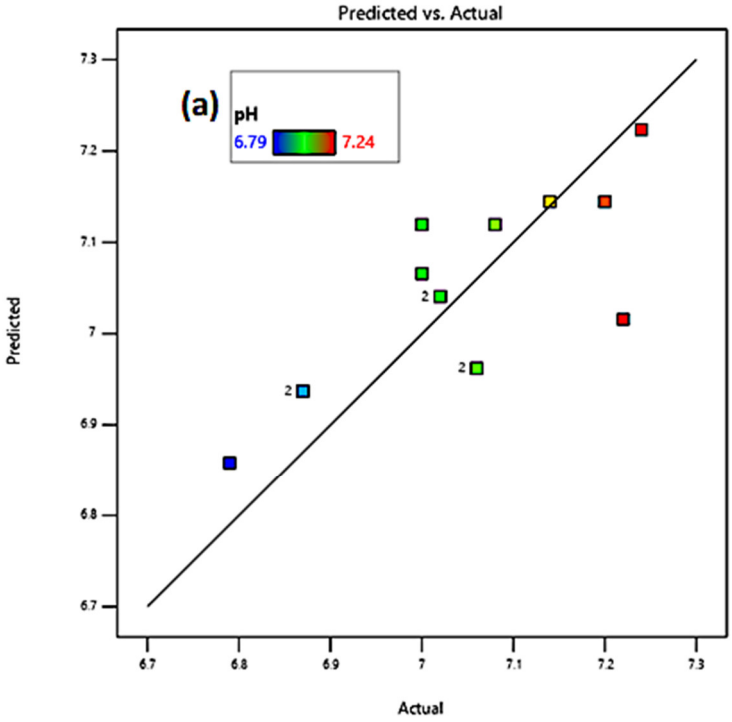
Predicted vs. Actual
(a)
pH
6.79
7.24
Predicted
Actual
6.7
6.8
6.9
7
7.1
7.2
7.3

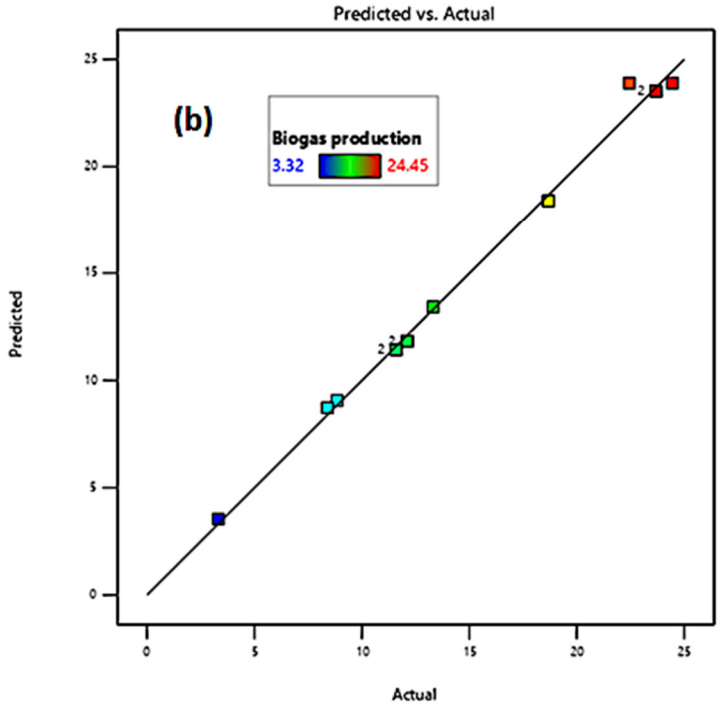
Predicted vs. Actual
(b)
Biogas production
3.32
24.45
Predicted
Actual
0
5
10
15
20
25

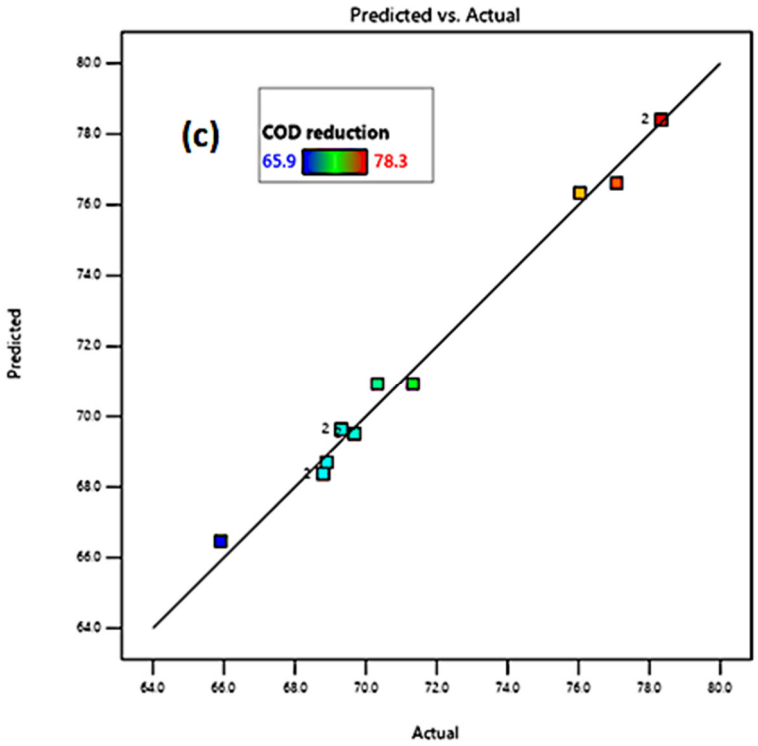

Figure 3. Predicted and experimental results of (**a**) pH, (**b**) biogas production, and (**c**) COD reduction.

3.2.1. ANOVA

The analysis of variance (ANOVA) indicated that the model-obtained results were statistically significant with a *p*-value less than 0.005. The F-value indicates that the lack of fit was not significant, which is desirable for the model to be justifiable. Tables 2–4 show results obtained from the ANOVA carried out using CCD-RSM to ascertain the significance and adequacy of the response models. The significance of the models' terms and their fitness were verified using the correlation coefficient (R^2) and the *p*-value for lack of fit. Meanwhile, the value of Prob > F relating to the lack of fit indicated that the model was not significant relative to the pure error. The coefficient of variance (CV%) indicated a high reliability of the experimental data with a high level of accuracy. The best fit for the models had a coefficient of determination (R^2) of pH (0.978), biogas production (0.995), and COD removal (0.992) closer to 1. It was deduced that the difference between the predicted and adjusted R^2 values was less than 0.2, which suggested that the response variable was predictively agreeable [45].

Table 2. Analysis of variance of pH response.

Source	Sum of Squares	df	Mean Square	F-Value	*p*-Value	
Model	0.2296	7	0.0328	38.39	0.0001	significant
A-Nano	0.0363	1	0.0363	42.53	0.0006	
B-Biochar loading rate	0.0002	1	0.0002	0.2399	0.6417	
AB	0.0092	1	0.0092	10.82	0.0166	
A^2	0.0525	1	0.0525	61.47	0.0002	
B^2	0.0215	1	0.0215	25.2	0.0024	
A^2B	0.063	1	0.063	73.77	0.0001	
AB^2	0.0171	1	0.0171	20.03	0.0042	
Residual	0.0051	6	0.0009			
Lack of Fit	0.0001	1	0.0001	0.125	0.7381	not significant
Pure Error	0.005	5	0.001			

Cor Total	0.2347	13		
Std. Dev. 0.0292	Mean 7.04		C.V% 0.415	Adeq Precision 20.37
R^2 0.978	Adjusted R^2 0.953			Predicted R^2 0.886

Table 3. Analysis of variance in biogas production response.

Source	Sum of Squares	df	Mean Square	F-Value	*p*-Value	
Model	579.59	5	115.92	305.25	<0.0001	significant
A-Nano	61.33	1	61.33	161.49	<0.0001	
B-Biochar loading rate	492.89	1	492.89	1297.94	<0.0001	
AB	22.77	1	22.77	59.96	<0.0001	
A^2	28.69	1	28.69	75.54	<0.0001	
B^2	501.5	1	501.5	1320.62	<0.0001	
Residual	3.04	8	0.3797			
Lack of Fit	1.04	3	0.346	0.865	0.5171	not significant
Pure Error	2	5	0.4			
Cor Total	582.62	13				
Std. Dev. 0.616	Mean 15.21		C.V% 4.05	Adeq Precision 50.44		
R^2 0.995	Adjusted R^2 0.992			Predicted R^2 0.986		

Table 4. Analysis of variance in COD reduction response.

Source	Sum of Squares	df	Mean Square	F-Value	*p*-Value	
Model	213.29	5	42.66	189.59	<0.0001	significant
A-Nano	9.12	1	9.12	40.52	0.0002	
B-Biochar loading rate	51.87	1	51.87	230.51	<0.0001	
AB	0.9604	1	0.9604	4.27	0.0727	
A^2	12.35	1	12.35	54.9	<0.0001	
B^2	30.5	1	30.5	135.56	<0.0001	
Residual	1.8	8	0.225			
Lack of Fit	1.3	3	0.4333	4.33	0.0741	not significant
Pure Error	0.5	5	0.1			
Cor Total	215.09	13				
Std. Dev. 0.47	Mean 71.56		C.V% 0.663	Adeq Precision 38.47		
R^2 0.992	Adjusted R^2 0.986			Predicted R^2 0.956		

3.2.2. Graphical Response of Input Factor Interaction

Three-dimensional (3D) response surface plots (Figure 4) revealed the visualization of the interaction effect of the input variables on the output responses. This was carried out by varying the input variables within the ranges to obtain a high peak. It was deduced that with a high nanoparticle load (A) of 0.6 g and a biochar load (B) of 1.5 mgVS/L, a high pH of 7.14 was achieved (Figure 4). This correlated to the fact that decreasing the AB load had a significant impact on the ionic binding of the substrate and the acidogenic and methanogenic activities about biogas production. Thus, a nanoparticle load (A) of the range 0.3–0.6 g and a biochar load (B) of the range 0.9–1.2 mgVS/L resulted in the highest biogas production at a level of 24 mL/day (Figure 4). On the other hand, the lower load of biochar (B) at 0.5 mgVS/L within any load of the nanoparticle (A) in a range of 0.2–0.6 g resulted in 78% COD removal. The effectiveness of lower proportions of the biochar might be due to the inadequate availability of pollutant molecules to absorb the excess active surface of the biochar at higher loads (B > 0.5 mgVS/L) [48,49]. The above trend was also in agreement with the result obtained by [20,49].

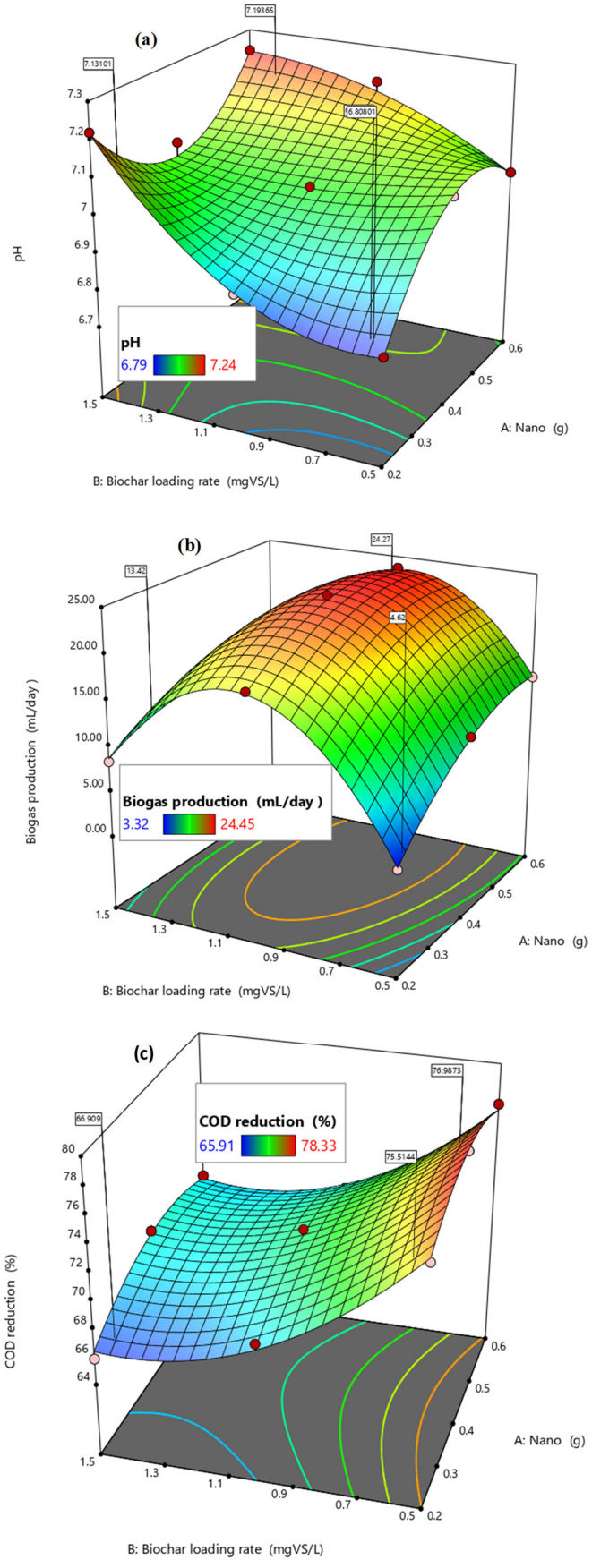

Figure 4. Three-dimensional (3D) response surface plots (**a**) pH, (**b**) biogas production, and (**c**) COD reduction.

3.3. Numerical Optimisation

To determine the stability of wastewater digestion as a function of pH, biogas production, and COD removal, without interruption. The mathematical models obtained from the simulated experimental data were found useful as predictive and monitoring tools to detect inhibition threats. The CCD numerical optimization provided a feasible solution to operate the system at optimum conditions. Thus, the optimization criteria were set to maximize the desirability efficiency within the range of the operating parameters. Figure 5 illustrates the selected ramp plot of the optimum parameters identified at a mesophilic temperature (37 °C) for 28 days. Even though there were 100 optimal solutions obtained, the selection of the optimum combination represents the multi-objective set with an overall desirability of 100%. Additional optimal solutions obtained to maximize the biogas production, COD removal, and pH stability are presented as supplementary data (Table S1). The set of constraints could change based on the process' objectives and desirability. According to the simulated scenario results shown in Table 5, the nanoparticle load (0.46 g), biochar load (0.66 mgVS/L), and pH (7.07) show 100% desirability performance. The response surface (contour and 3-D) plots (Figure 4), in conjunction with the ramp plot (Figure 5), can be used to see the best region and confirm the model-predicted results. The quadratic second-order models' vital maximums, minimums, or saddles are possible definitions for their critical points.

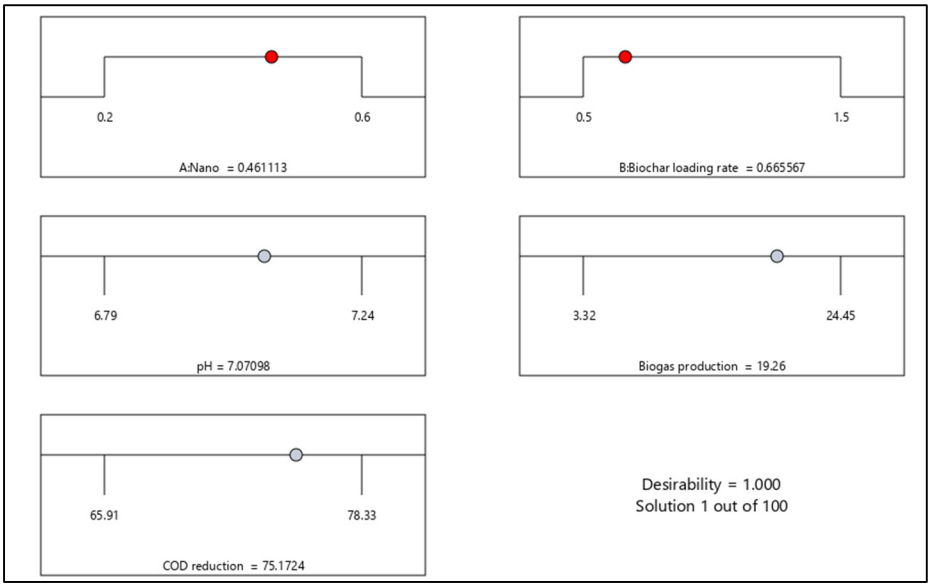

Figure 5. Ramp plot of the optimization result of methane production and COD reduction.

Table 5. Selected optimized conditions.

Number	Nanoparticle Load (g)	Biochar Loading (mgVS/L)	pH	Biogas (mL/day)	COD Removal (mg/L)	Desirability
1	0.46	0.66	7.07	19.26	75.17	1
2	0.4	1.5	7.04	11.83	69.5	1
3	0.6	1	7.17	23.51	69.63	1
4	0.4	1	7.01	23.89	70.93	1
5	0.4	0.5	7.06	11.4	78.4	1
6	0.2	1	6.87	18.41	68.37	1
7	0.6	1.5	7.23	9.06	68.7	1
8	0.2	1.5	7.21	8.72	66.46	1
9	0.6	0.5	6.99	13.42	76.62	1
10	0.26	0.5	6.9	6.5	77.26	1

4. Conclusions

In this study, the matrix of the experimental runs was determined using the central composite design (CCD) of the response surface methodology (RSM). This supported the data screening, designing, optimization, model testing, and validation of the results obtained and the determination of the multifunctional impact of the input variables. Thus, the modelled experimental data provided reasonable prediction performance of a bio-stimulated AD process with nanoparticle and biochar additives. The synergistic effect of additives resulted in over 70% degradability of the wastewater. RSM results revealed that the methanogenesis phase and stability of the wastewater biodegrading moved toward a neutral pH. At constant temperature (37 °C) and HRT (28 days), the optimized load of nanoparticles (0.46 g) and biochar (0.66 mgVS/L) resulted in a biogas production of 19.26 mL/day, a pH of 7.07, and a COD removal of 75.17%. This established the trade-off between biogas productivity, biodegradability, and the stability of an AD process operation. Moreover, this result requires the consideration of the use of nanoparticles as a bio-stimulant to build up the process for commercialization in the future.

Supplementary Materials: The following are available online at https://www.mdpi.com/article/10.3390/app122312037/s1, Table S1: Central composite design optimized conditions.

Author Contributions: Conceptualisation E.K.T. and J.A.A.; writing—original draft G.A.-D. and J.A.A.; writing-reviewing and editing E.K.T., E.K.A. and S.R.; supervision S.R. and M.C.; Administration E.K.T. All authors have read and agreed to the published version of the manuscript with no conflict of interest.

Funding: This research received no external funding.

Institutional Review Board Statement: Not applicable.

Informed Consent Statement: Not applicable.

Data Availability Statement: Not applicable.

Acknowledgments: The authors would like to thank the Green Engineering Research Group, under the Department of Chemical Engineering Department of the Durban University of Technology, South Africa, for their support.

Conflicts of Interest: The authors state that they have no recognized competing financial or personal interests that might have influenced the work presented in this publication.

References

1. Zamri, M.; Hasmady, S.; Akhiar, A.; Ideris, F.; Shamsuddin, A.; Mofijur, M.; Fattah, I.R.; Mahlia, T. A comprehensive review on anaerobic digestion of organic fraction of municipal solid waste. *Renew. Sustain. Energy Rev.* **2021**, *137*, 110637.
2. Tetteh, E.K.; Rathilal, S.; Chetty, M.; Armah, E.K.; Asante-Sackey, D. Treatment of water and wastewater for reuse and energy generation-emerging technologies. In *Water and Wastewater Treatment*; IntechOpen: London, UK, 2019; pp. 53–80.
3. Stronach, S.M.; Rudd, T.; Lester, J.N. *Anaerobic Digestion Processes in Industrial Wastewater Treatment*; Springer Science & Business Media: Berlin/Heidelberg, Germany, 2012.
4. Baloch, H.A.; Nizamuddin, S.; Siddiqui, M.T.H.; Riaz, S.; Jatoi, A.S.; Dumbre, D.K.; Mubarak, N.; Srinivasan, M.; Griffin, G. Recent advances in production and upgrading of bio-oil from biomass: A critical overview. *J. Environ. Chem. Eng.* **2018**, *6*, 5101–5118.
5. Zhu, X.; Blanco, E.; Bhatti, M.; Borrion, A. Impact of metallic nanoparticles on anaerobic digestion: A systematic review. *Sci. Total Environ.* **2020**, *757*, 143747.
6. Xu, Q.; Li, W.; Ma, L.; Cao, D.; Owens, G.; Chen, Z. Simultaneous removal of ammonia and phosphate using green synthesized iron oxide nanoparticles dispersed onto zeolite. *Sci. Total Environ.* **2020**, *703*, 135002.
7. Aragaw, T.A.; Bogale, F.M.; Aragaw, B.A.; Aragaw, B.A. Iron-based nanoparticles in wastewater treatment: A review on synthesis methods, applications, and removal mechanisms. *J. Saudi Chem. Soc.* **2021**, *25*, 101280.
8. Yang, J.; Hou, B.; Wang, J.; Tian, B.; Bi, J.; Wang, N.; Li, X.; Huang, X. Nanomaterials for the removal of heavy metals from wastewater. *Nanomaterials* **2019**, *9*, 424.
9. Ali, A.; Zafar, H.; Zia, M.; ul Haq, I.; Phull, A.R.; Ali, J.S.; Hussain, A. Synthesis, characterization, applications, and challenges of iron oxide nanoparticles. *Nanotechnol. Sci. Appl.* **2016**, *9*, 49–67.
10. Yang, Y.; Zhang, C.; Hu, Z. Impact of metallic and metal oxide nanoparticles on wastewater treatment and anaerobic digestion. *Environ. Sci. Process. Impacts* **2013**, *15*, 39–48.

11. Suanon, F.; Sun, Q.; Mama, D.; Li, J.; Dimon, B.; Yu, C.-P. Effect of nanoscale zero-valent iron and magnetite (Fe_3O_4) on the fate of metals during anaerobic digestion of sludge. *Water Res.* **2016**, *88*, 897–903.
12. Engliman, N.S.; Abdul, P.M.; Wu, S.-Y.; Jahim, J.M. Influence of iron (II) oxide nanoparticle on biohydrogen production in thermophilic mixed fermentation. *Int. J. Hydrogen Energy* **2017**, *42*, 27482–27493.
13. Liu, Y.; Wang, Q.; Zhang, Y.; Ni, B.-J. Zero valent iron significantly enhances methane production from waste activated sludge by improving biochemical methane potential rather than hydrolysis rate. *Sci. Rep.* **2015**, *5*, 8263.
14. Melikoglu, M. Reutilisation of food wastes for generating fuels and value added products: A global review. *Environ. Technol. Innov.* **2020**, *19*, 101040.
15. AlNouss, A.; Parthasarathy, P.; Mackey, H.R.; Al-Ansari, T.; McKay, G. Pyrolysis study of different fruit wastes using an Aspen Plus Model. *Front. Sustain. Food Syst.* **2021**, *5*, 4.
16. Tan, X.-F.; Liu, Y.-G.; Gu, Y.-L.; Xu, Y.; Zeng, G.-M.; Hu, X.-J.; Liu, S.-B.; Wang, X.; Liu, S.-M.; Li, J. Biochar-based nano-composites for the decontamination of wastewater: A review. *Bioresour. Technol.* **2016**, *212*, 318–333.
17. Tan, X.-F.; Liu, S.-B.; Liu, Y.-G.; Gu, Y.-L.; Zeng, G.-M.; Hu, X.-J.; Wang, X.; Liu, S.-H.; Jiang, L.-H. Biochar as potential sustainable precursors for activated carbon production: Multiple applications in environmental protection and energy storage. *Bioresour. Technol.* **2017**, *227*, 359–372.
18. Ahmad, T.; Danish, M.; Rafatullah, M.; Ghazali, A.; Sulaiman, O.; Hashim, R.; Ibrahim, M.N.M. The use of date palm as a potential adsorbent for wastewater treatment: A review. *Environ. Sci. Pollut. Res.* **2012**, *19*, 1464–1484.
19. Liang, Y.; Cao, X.; Zhao, L.; Xu, X.; Harris, W. Phosphorus release from dairy manure, the manure-derived biochar, and their amended soil: Effects of phosphorus nature and soil property. *J. Environ. Qual.* **2014**, *43*, 1504–1509.
20. Dugdug, A.A.; Chang, S.X.; Ok, Y.S.; Rajapaksha, A.U.; Anyia, A. Phosphorus sorption capacity of biochars varies with biochar type and salinity level. *Environ. Sci. Pollut. Res.* **2018**, *25*, 25799–25812.
21. Sousa, A.; Figueiredo, C. Sewage sludge biochar: Effects on soil fertility and growth of radish. *Biol. Agric. Hortic.* **2016**, *32*, 127–138.
22. Sanchez-Monedero, M.; Cayuela, M.; Roig, A.; Jindo, K.; Mondini, C.; Bolan, N. Role of biochar as an additive in organic waste composting. *Bioresour. Technol.* **2018**, *247*, 1155–1164.
23. Liu, L.; Fan, S. Removal of cadmium in aqueous solution using wheat straw biochar: Effect of minerals and mechanism. *Environ. Sci. Pollut. Res.* **2018**, *25*, 8688–8700.
24. Pan, J.; Ma, J.; Zhai, L.; Luo, T.; Mei, Z.; Liu, H. Achievements of biochar application for enhanced anaerobic digestion: A review. *Bioresour. Technol.* **2019**, *292*, 122058.
25. Dudek, M.; Świechowski, K.; Manczarski, P.; Koziel, J.A.; Białowiec, A. The effect of biochar addition on the biogas production kinetics from the anaerobic digestion of brewers' spent grain. *Energies* **2019**, *12*, 1518.
26. Lü, F.; Luo, C.; Shao, L.; He, P. Biochar alleviates combined stress of ammonium and acids by firstly enriching *Methanosaeta* and then *Methanosarcina*. *Water Res.* **2016**, *90*, 34–43.
27. Luo, C.; Lü, F.; Shao, L.; He, P. Application of eco-compatible biochar in anaerobic digestion to relieve acid stress and promote the selective colonization of functional microbes. *Water Res.* **2015**, *68*, 710–718.
28. Shen, Y.; Forrester, S.; Koval, J.; Urgun-Demirtas, M. Yearlong semi-continuous operation of thermophilic two-stage anaerobic digesters amended with biochar for enhanced biomethane production. *J. Clean. Prod.* **2017**, *167*, 863–874.
29. American Public Health Association (APHA). *Standard Methods for the Examination of Water and Wastewater*; American Public Health Association (APHA): Washington, DC, USA, 2012. Available online: https://www.standardmethods.org/doi/book/10.2105/SMWW.2882?gclid=CjwKCAiA25v_BRBNEiwAZb4-ZRdKz6ceq6 (accessed on 19 October 2022).
30. Tetteh, E.K.; Amo-Duodu, G.; Rathilal, S. Synergistic Effects of Magnetic Nanomaterials on Post-Digestate for Biogas Production. *Molecules* **2021**, *26*, 6434. https://doi.org/10.3390/molecules26216434.
31. Amo-Duodu, G.; Tetteh, E.K.; Rathilal, S.; Armah, E.K.; Adedeji, J.; Chollom, M.N.; Chetty, M. Effect of Engineered Biomaterials and Magnetite on Wastewater Treatment: Biogas and Kinetic Evaluation. *Polymers* **2021**, *13*, 4323. https://doi.org/10.3390/polym13244323.
32. El Ghandoor, H.; Zidan, H.; Khalil, M.M.; Ismail, M. Synthesis and some physical properties of magnetite (Fe_3O_4) nanoparticles. *Int. J. Electrochem. Sci.* **2012**, *7*, 5734–5745.
33. Mascolo, M.C.; Pei, Y.; Ring, T.A. Room temperature co-precipitation synthesis of magnetite nanoparticles in a large pH window with different bases. *Materials* **2013**, *6*, 5549–5567.
34. Ghaleb, A.A.S.; Kutty, S.R.M.; Ho, Y.-C.; Jagaba, A.H.; Noor, A.; Al-Sabaeei, A.M.; Almahbashi, N.M.Y. Response surface methodology to optimize methane production from mesophilic anaerobic co-digestion of oily-biological sludge and sugarcane bagasse. *Sustainability* **2020**, *12*, 2116.
35. Khumalo, S.M.; Bakare, B.F.; Rathilal, S.; Tetteh, E.K. Characterization of South African Brewery Wastewater: Oxidation-Reduction Potential Variation. *Water* **2022**, *14*, 1604.
36. Kweinor Tetteh, E.; Rathilal, S. Biogas production from wastewater treatment-evaluating anaerobic and biomagnetic systems. *Water-Energy Nexus* **2021**, *4*, 165–173. https://doi.org/10.1016/j.wen.2021.11.004.
37. Madondo, N.I.; Tetteh, E.K.; Rathilal, S.; Bakare, B.F. Synergistic Effect of Magnetite and Bioelectrochemical Systems on Anaerobic Digestion. *Bioengineering* **2021**, *8*, 198. https://doi.org/10.3390/bioengineering8120198.

38. El-Gendy, N.S.; Nassar, H.N. Biosynthesized magnetite nanoparticles as an environmental opulence and sustainable wastewater treatment. *Sci. Total Environ.* **2021**, *774*, 145610.
39. Zhao, J.; Li, Y.; Dong, R. Recent progress towards in-situ biogas upgrading technologies. *Sci. Total Environ.* **2021**, *800*, 149667. https://doi.org/10.1016/j.scitotenv.2021.149667.
40. Godvin Sharmila, V.; Rajesh Banu, J.; Gunasekaran, M.; Angappane, S.; Yeom, I.T. Nano-layered TiO_2 for effective bacterial disintegration of waste activated sludge and biogas production. *J. Chem. Technol. Biotechnol.* **2018**, *93*, 2701–2709.
41. Durán, I.; Rubiera, F.; Pevida, C. Modeling a biogas upgrading PSA unit with a sustainable activated carbon derived from pine sawdust. Sensitivity analysis on the adsorption of CO_2 and CH_4 mixtures. *Chem. Eng. J.* **2022**, *428*, 132564.
42. Ángeles, R.; Vega-Quiel, M.J.; Batista, A.; Fernández-Ramos, O.; Lebrero, R.; Muñoz, R. Influence of biogas supply regime on photosynthetic biogas upgrading performance in an enclosed algal-bacterial photobioreactor. *Algal Res.* **2021**, *57*, 102350.
43. Abdelsalam, E.; Samer, M.; Attia, Y.; Abdel-Hadi, M.; Hassan, H.; Badr, Y. Comparison of nanoparticles effects on biogas and methane production from anaerobic digestion of cattle dung slurry. *Renew. Energy* **2016**, *87*, 592–598.
44. Manmai, N.; Unpaprom, Y.; Ramaraj, R. Bioethanol production from sunflower stalk: Application of chemical and biological pretreatments by response surface methodology (RSM). *Biomass Convers. Biorefinery* **2021**, *11*, 1759–1773.
45. Chollom, M.N.; Bakare, B.F.; Rathilal, S.; Tetteh, E.K. Evaluating the Biodegradation of Veterinary Antibiotics Using Kinetics Model and Response Surface Methodology. *Molecules* **2022**, *27*, 5402.
46. Abdulhameed, A.S.; Mohammad, A.-T.; Jawad, A.H. Application of response surface methodology for enhanced synthesis of chitosan tripolyphosphate/TiO_2 nanocomposite and adsorption of reactive orange 16 dye. *J. Clean. Prod.* **2019**, *232*, 43–56.
47. Apollo, S.; Onyango, M.S.; Ochieng, A. Modelling energy efficiency of an integrated anaerobic digestion and photodegradation of distillery effluent using response surface methodology. *Environ. Technol.* **2016**, *37*, 2435–2446.
48. Chen, Y.; Cheng, J.J. Effect of potassium inhibition on the thermophilic anaerobic digestion of swine waste. *Water Environ. Res.* **2007**, *79*, 667–674.
49. Wu, L.-J.; Kobayashi, T.; Kuramochi, H.; Li, Y.-Y.; Xu, K.-Q. Effects of potassium, magnesium, zinc, and manganese addition on the anaerobic digestion of de-oiled grease trap waste. *Arab. J. Sci. Eng.* **2016**, *41*, 2417–2427.